

AperTO - Archivio Istituzionale Open Access dell'Università di Torino

Charge trapping in TiO₂ polymorphs as seen by Electron Paramagnetic Resonance Spectroscopy

This is the author's manuscript

Original Citation:

Availability:

This version is available <http://hdl.handle.net/2318/139998> since

Terms of use:

Open Access

Anyone can freely access the full text of works made available as "Open Access". Works made available under a Creative Commons license can be used according to the terms and conditions of said license. Use of all other works requires consent of the right holder (author or publisher) if not exempted from copyright protection by the applicable law.

(Article begins on next page)



UNIVERSITÀ DEGLI STUDI DI TORINO

This is an author version of the contribution published on:

Questa è la versione dell'autore dell'opera:

Phys.Chem. Chem. Phys., 2013, **15**, 9435, DOI: 10.1039/c3cp50658d

Mario Chiesa, Maria Cristina Paganini, Stefano Livraghi and Elio Giamello

The definitive version is available at:

La versione definitiva è disponibile alla URL:

www.rsc.org/pccp

Charge trapping in TiO₂ polymorphs as seen by Electron Paramagnetic Resonance Spectroscopy.

Mario Chiesa, Maria Cristina Paganini, Stefano Livraghi and Elio Giamello*

Dipartimento di Chimica and NIS. Università di Torino. Via P. Giuria 7. 10125 Torino.

Abstract.

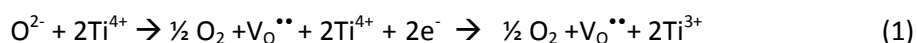
Electron Paramagnetic Resonance techniques (EPR) have been employed to investigate charge carriers trapping in the two main TiO₂ polymorphs, anatase and rutile, with particular attention to the features of electron trapping sites (formally Ti³⁺ ions). The classic CW-EPR technique in this case provides signals based on the g tensor only. Nevertheless a systematic analysis of the signals obtained in the various cases (anatase and rutile, surface and bulk centers, regular and defective sites) have been performed providing useful guidelines in a field affected by some confusion. The problem of the localization of the electron spin density have been tackled by means of Pulse-EPR hyperfine techniques on samples appositely enriched with ¹⁷O. This approach has led to evidence a substantial difference, in terms of wavefunction localization between anatase (electrons trapped in regular lattice sites exhibiting delocalized electron density) and rutile (interstitial sites showing localized electron density).

1. Introduction.

Titanium dioxide (or titania) is a solid material with a Janus-faced character, showing two distinct and somehow opposite faces. The first one is that of a material useful for several large scale practical applications. More than four millions tons of TiO₂ are prepared per year, to be used, as a white and opaque pigment, in conventional applications such as paintings, food additives, cosmetics, toothpastes, drugs, paper and plastics. The second face of titanium dioxide is that of a sophisticated functional material attractive for advanced applications among which photochemistry is probably the most prominent. Since the fundamental discovery of water photosplitting under UV irradiation in 1972¹, titanium dioxide is considered an efficient photocatalyst^{2,3} and is used in reactions for mineralization of water and air pollutants⁴. Later, titanium dioxide has been employed in photochemical processes as bactericide^{5,6} in photokilling of tumor cells⁵, in odour control⁷, and as a superhydrophilic antifogging agent⁸. Additionally, in recent years, the use of titanium dioxide in solar energy conversion processes based on dye sensitization of the solid has become very important.⁹ The photocatalytic applications listed above (except for the dye sensitisation which follows a particular route) have a common starting point. Irradiation of a crystal of the oxide entails the initial excitation event followed by charge spatial separation. This leads to the promotion of an electron (e⁻) in conduction band (CB) and the formation of an electron hole (or hole, h⁺) in the valence band (VB). The initial light induced separation is followed by charge migration to the surface, charge trapping and, eventually, charge transfer to adsorbed entities^{10, 11}. All the above steps are the object of often sophisticated investigations and are still not yet fully understood. In particular the nature of the charge traps, their location (surface, subsurface, bulk), the stability of the trapped charge and their propensity to detrapping are all issues of vital importance.

The surface of the solid is deeply involved in its photoactivity and it is therefore not surprising that titanium dioxide has been widely investigated under the point of view of the surface science as reviewed in some extensive review papers^{12,13,14}. Very intense is, in parallel, the computational activity aimed to explore the structure of the surface^{15, 16} and the phenomena of charge transport¹⁷ and stabilisation¹⁸.

Trapped electrons and trapped holes can form in TiO₂ also because of chemical modifications of the solid. Titanium dioxide in fact belongs to the class of reducible oxides as it easily loses oxygen upon annealing under vacuum with formation of oxygen vacancies (V_O^{••} is an empty vacancy in the Kröger-Vink notation) and, in parallel, of excess electrons.



Loosing oxygen the insulating oxide becomes a n-type semiconductor. Excess electrons generated by the oxygen depletion are stabilized into the reduced solid and deeply influence its chemical and physical properties including catalytic and photocatalytic ones. Although, as pointed out by M. H. Henderson in its recent review paper¹⁴, some caution must be taken when comparing excess electrons (or holes) formed because an alteration of the oxide stoichiometry with those due to photoexcitation, the study and the

classification of trapping sites in the various TiO_2 polymorphs is undoubtedly very useful. The principal and most investigated polymorphs of titanium dioxide are rutile (R, the thermodynamically stable phase) and anatase (A) while less explored are the properties of brookite (B). All three polymorphs are built up by distorted octahedral TiO_6 units connected by corner and edge sharing and differing in the arrangement of the various interconnections. All oxygen are surrounded by three Ti ions (OTi_3). The two main polymorphs have similar band gap energy (3.0 eV and 3.2 eV for R and A respectively) and differ in terms of the more stable crystal faces which are the (110) in the case of rutile and the (101) in the case of anatase. The relatively small difference between anatase and rutile cause however important distinctions in their behaviour. In particular anatase is more active in photocatalytic terms than rutile even though the maximum photocatalytic activity is usually observed in the case of P25, a mixed phase system produced by Degussa, whose peculiar properties have been recently discussed in terms of an active interface between A and R phases which would favour the spatial separation of the photo-generated charges¹⁹. Since rutile is the most thermodynamically stable polymorph and its single crystals are easily available, this phase has long been the most investigated one by Surface Science while anatase, due to its better photocatalytic performances, has been more considered in applied photocatalysis studies and, consequently, in characterisation activities using polycrystalline solids. This has caused therefore a certain imbalance in the literature in particular for the relatively poor number of single crystal studies on anatase.

When excess electrons are generated in Titania they are usually stabilized by metal cations with formation of Ti^{3+} units (second part of equation 1). In spite of the fact that, in some cases, the presence of electrons trapped in oxygen vacancies has been invoked (mainly on the basis of optical absorption²⁰) unambiguous evidence about the presence such a centres (color centres or F centres) in titanium dioxide has, in our opinion, never been provided. Moreover modern and accurate theoretical calculation firmly indicate that electrons released in the solid by oxygen depletion are preferentially stabilized on Ti d orbitals²¹.

Actually the presence of Ti^{3+} in reduced or in irradiated TiO_2 is well documented by EELS²², polarized optical spectroscopy²³, photoelectron spectroscopy²⁴ and, in particular by Electron Paramagnetic Resonance (EPR)²⁵ which is the main technique adopted in our group to investigate bulk and surface defects in solids and radical intermediates at solid surfaces.^{26,27} EPR techniques are, beyond any doubt, the reference techniques for detection of radicals and, in general, of paramagnetic species. The advantages of EPR, beside its specificity, are more than one. In particular EPR is highly sensitive, it provides information on the symmetry of the paramagnetic centre and, in the case of presence of nuclei having non zero nuclear spin interacting with the unpaired electron, it allows detailed mapping of the electron spin density via the so called hyperfine interaction. A further advantage, particularly useful in the studies of oxides photochemistry, is the low frequency of the electromagnetic radiation needed for electron spin resonance (in the range of microwaves) which allows recording EPR spectra either in dark or under irradiation with higher frequency light (UV, visible, infrared) without interference, thus increasing the number of

experimental opportunities. The EPR technique has been used, on the one hand, in studies of excess electrons in rutile single crystals^{25c,f, 28,29,30} mainly aimed to understand the symmetry of Ti^{3+} centres. On the other hand investigations on polycrystalline TiO_2 systems can be divided in two types i.e. those mainly devoted to phenomenological aspects of the oxide behaviour and of its surface chemistry (formation of reduced Ti^{3+} centres in various conditions, reactivity with adsorbates etc.) and those aiming to elucidate the effect of the solid irradiation in terms of charge trapping and surface charge transfer^{19, 31}. In spite of this considerable experimental effort, however, several questions concerning the nature and location (surface or bulk, lattice or interstitial) of the centres detected by EPR for the various polymorphs remain open. In particular a conclusive assignment of each EPR signal observed in TiO_2 to a well-defined centre is still incomplete. Additionally, a fundamental question which remains open and is the focus of a lively debate is related to the nature of the electronic states associated to excess electrons in Titania whose wave function has been already described either as localized on a single titanium ion or delocalized over several of them. This problem has been tackled by several groups using sophisticated experimental approaches such as resonant photoelectron diffraction³² or STM³³ and by a number of theoretical investigations. EPR, till little time ago, did not contribute to this debate because of the absence of hyperfine structure in the spectra of both trapped electrons and trapped holes. As it will be clarified in next Sections the first EPR data on hyperfine interactions in TiO_2 are now appearing in the literature thanks to the techniques of enrichment of the solid with suitable isotopes (*vide infra*).

The present paper is devoted to a survey of EPR results from our laboratory on trapped charge carriers (mainly excess electrons) in TiO_2 with the aim of rationalizing the somehow blurred picture today available with convincing assignments. In particular we aim to distinguish the behaviour of the two main polymorphs and to illustrate the various ways to generate trapped electrons and holes in the solid. For the sake of simplicity we refrain to discuss in this paper the results obtained on non-metal-doped titanias, in particular N- TiO_2 and related systems, using a similar approach³⁴. Doped titania are studied mainly to obtain solids showing photoactivity under visible light. The bulk of concepts and results recently produced in this particular field are large enough to deserve a specific discussion.

2. Materials and methods

The studies accounted in the present paper were performed on TiO_2 prepared via various distinct procedures. In the case of anatase we have carried out two types of sol-gel preparations via hydrolysis of titanium (IV) isopropoxide and of $TiCl_4$ respectively. Details on these preparations have been reported elsewhere. The dried material after hydrolysis were heated at 773 K in air for different time intervals. Another type of anatase was prepared by Chemical Vapour Reaction by oxidation of Titanium isopropoxide vapours in a home made flow reactor. The resulting powders were characterized by X-Ray diffraction, surface area measurements and Transmission Electron Microscopy. Figure 1 reports TEM pictures of the

four anatase samples considered in the present investigation. The morphological features of the same samples are reported in Table 1.

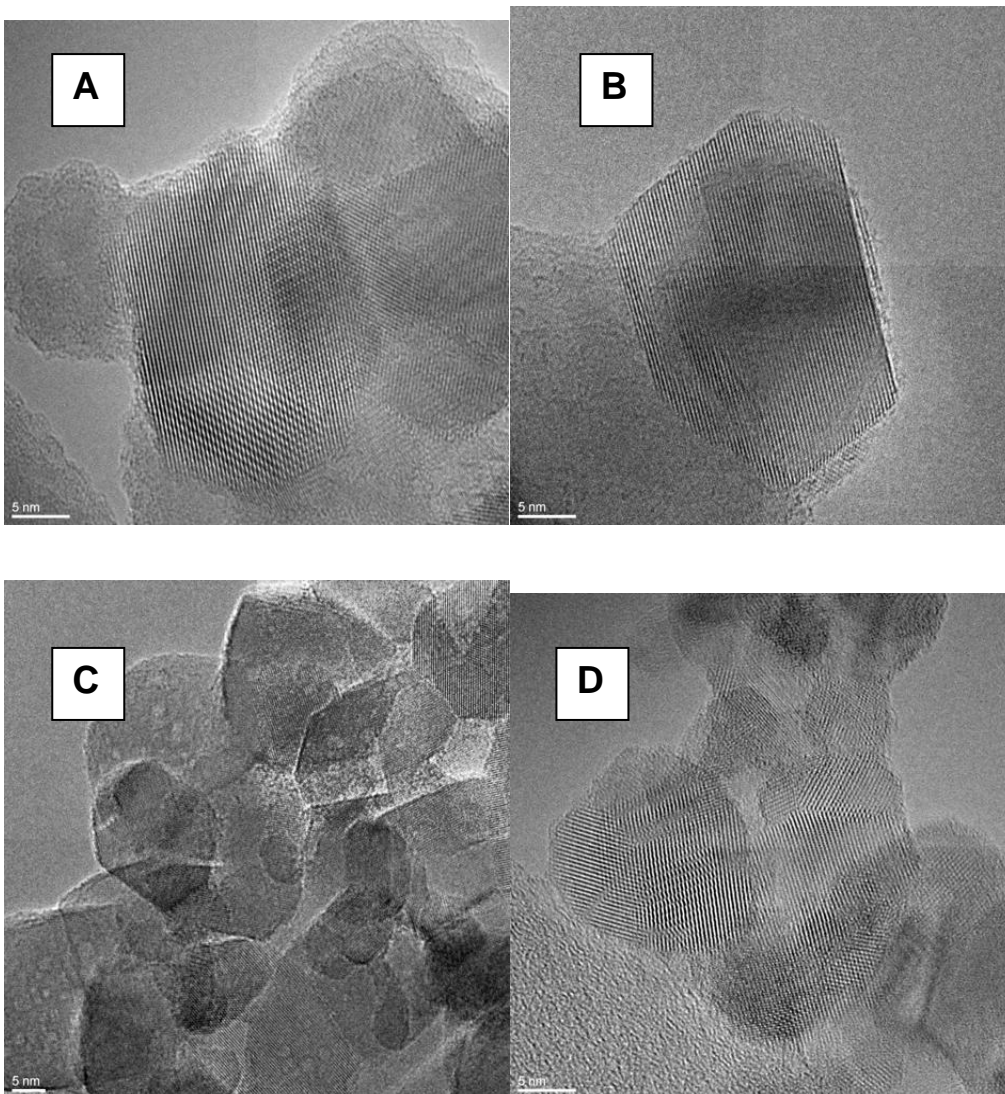


Figure 1. TEM images of four differently prepared anatase materials. A) prepared by sol gel of Ti isopropoxide and successive calcination at 773K for 1 hour. B) prepared by sol gel of Ti isopropoxide and successive calcination at 773K for 24 hours. C) prepared by hydrolysis of TiCl_4 and successive calcination for 1h. D) prepared by Chemical Vapor Reaction (CVR).

All experiments aimed to monitor the features of electron or hole trapping centres gave similar results for all the samples, the only difference being, in some case, a variation of the relative intensities of the EPR peaks of the various species. In quantitative terms the whole intensity of the signals showed moderate variations from case to case related to the crystal size.

Sample label (Figure 1)	Crystallographic Phase	Specific Surface Area/ $\text{m}^2 \text{g}^{-1}$ (B.E.T. method)	Average crystal size/nm (Rietveld refinement)
A	Anatase	21	47
B	Anatase	43	26
C	Anatase	24	46
D	Anatase	6	150

Table 1. Morphological features of the four anatase samples reported in Fig. 1.

Experiments on rutile were performed either on commercial powders (microrutile and nanorutile from Aldrich respectively) or on solids obtained by high temperature treatment of the anatase systems described before. Reduced (blue) rutile TiO_2 was prepared by hydrolysis of TiCl_4 with a stoichiometric amount of water under N_2 flow. The powder was kept under N_2 flow for 2 hours and successively transferred in a quartz tube and heated up to 973 K for 10 minutes under N_2 flow. ^{17}O enrichment of TiO_2 samples (anatase or rutile) was obtained by employing ^{17}O isotopically enriched water (40% ^{17}O enrichment supplied by Icon Services New Jersey).

3. Electron Paramagnetic Resonance and titanium dioxide: the g tensor of trapped electrons and holes

Conventional CW-EPR (Continuous Wave-EPR) has been until now largely dominant in titanium dioxide studies. In a CW-EPR experiment the substance under investigation interacts with a homogeneous magnetic field which is allowed to vary in a selected range and is irradiated by a continuous flow of microwaves at fixed frequency which, when resonance conditions are fulfilled, entails a transition between two spin states. Microwaves belonging to the X-band (about 9.5GHz) are the most commonly used even though in some case higher frequencies are useful to resolve particular spectra. A CW-EPR spectrum reports the first derivative of the microwave absorption as a function of the swept magnetic field measured in Tesla or in Gauss (1 Tesla = 10^4 Gauss). Pulse EPR (a method based on irradiation by short microwave pulses) were introduced more recently. However these techniques started to undergo rapid development and are now finding wider applications. For details on the principles of EPR techniques and applications to solid state and catalysis studies the reader is referred to recently published books or specialist reports^{35 36}. Ti^{3+} is paramagnetic ($S=1/2$) having a $3d^1$ configuration. In solid crystals the ground state of the free ion is

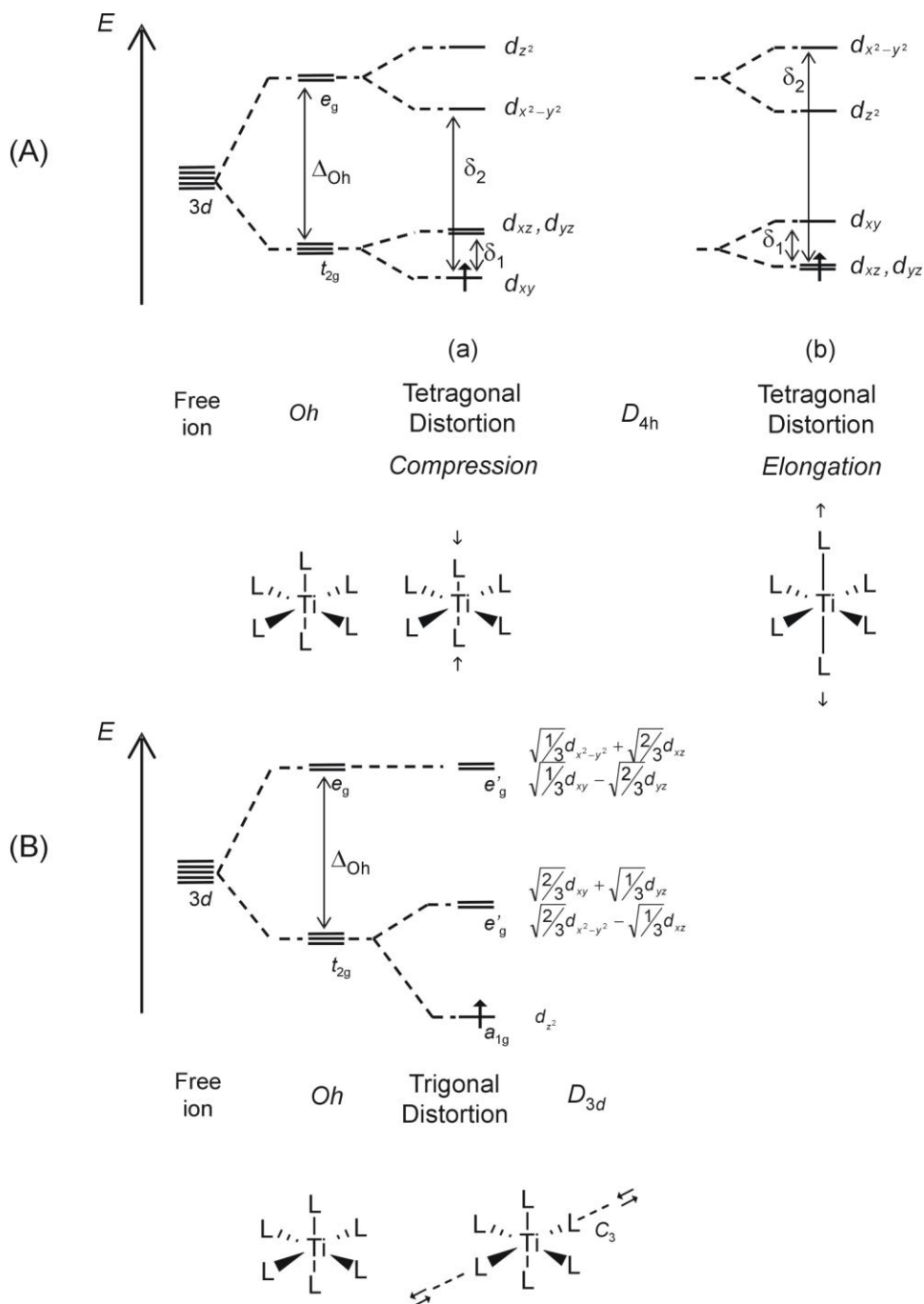
split by the effect of a crystal field. Since in all TiO₂ polymorphs the dominating symmetry is octahedral, we will limit our discussion exclusively to this case. When the metal ion is octahedrally coordinated, the free-ion ground state is split so to give two subgroups with three t_{2g} and two e_g orbitals separated by the energy term Δ_O. An additional tetragonal (Scheme1A) or trigonal (Scheme1B) distortion further lifts the degeneracy of the t_{2g} and e_g levels and results in anisotropic g values. In the tetragonal case (D_{4h}), if the distortion is a tetragonal compression, the ground state is the d_{xy} orbital (Scheme1A(a)), while if the distortion is a tetragonal elongation (Scheme1A(b)), the ground state is a degenerate d_{xy}, d_{yz} orbital. In the latter case, Ti³⁺ exhibits a Jahn-Teller effect that further resolves the degeneration. The g value expressions for a Ti³⁺ ion in a tetragonally distorted octahedral environment are:

$$g_{\parallel} \cong g_e - (8\lambda/\delta_2) \text{ and } g_{\perp} \cong g_e - (2\lambda/\delta_1) \quad \text{Eq. 1}$$

where δ₁ and δ₂ are the energy separation between the d-orbitals shown in Scheme 1A. In the case of trigonally distorted octahedral (D_{3d}) symmetry the five orbitals are split into three energy states, as shown in Scheme1B. We include this case for the sake of completeness, however trigonal distortions do not occur in TiO₂. The resulting d orbitals are quantized with respect to the three-fold axis, and the unpaired electron dwells in the d_{z²} orbital. The theoretical g values are:

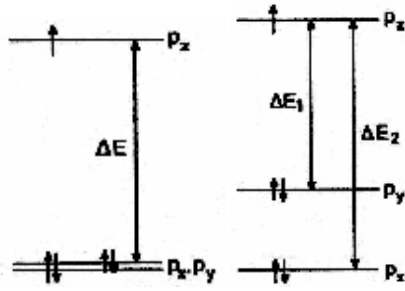
$$g_{\parallel} = g_e \text{ and } g_{\perp} = g_e - (2\lambda/\delta) \quad \text{Eq. 2}$$

Although CW-EPR can provide evidence for the local symmetry adopted by Ti³⁺ ions, the details of the metal to ligand interaction and the coordination geometry of first and second shells remain largely undetermined. Insights into this direction can be obtained by advanced EPR methods when isotopic enrichment in magnetically active isotopes is obtained. The main isotopes of Ti and O are ⁴⁸Ti and ¹⁶O both having nuclear spin I=0. The abundance of Ti magnetic isotopes i.e. ⁴⁷Ti (I=5/2 natural abundance 7.44%) and ⁴⁹Ti (I=7/2 natural abundance 5.41%) is, in most case of solid systems, not enough high to produce a detectable hyperfine structure. The same applies for ¹⁷O (I=5/2) whose natural abundance is only 0.037%. The information provided by the hyperfine structure, essential to monitor the localisation degree of the wavefunction, is therefore absent in the spectra of electrons and holes trapped in TiO₂ when the constituent elements are in natural abundance.



Scheme 1. Level scheme for the d -orbitals of Ti^{3+} undergoing (A) tetragonally and (B) trigonally distorted octahedral crystal field.

An electron hole at the surface of a metal oxide or in correspondence of a cation vacancy (in the second case the defect is known as V centre) localizes on oxide anions producing a paramagnetic centre which, in chemical terms, can be described as a O^- ion ($O^{2-} + h^+ \rightarrow O^-$) having the unpaired electron hosted in a 2p orbital. This fact is confirmed by both theoretical and experimental EPR results.³⁷ According to the symmetry of the environment the g tensor can result either axial or rhombic (Scheme 2)



Scheme 2. Energy levels of O^- ions in axial and rhombic symmetry.

The expected g values in the axial case is :

$$g_{||} = g_{zz} \approx g_e; \quad g_{\perp} = g_e + 2\lambda/\Delta E . \quad (5)$$

In rhombic symmetry one has:

$$g_{zz} \approx g_e; \quad g_{xx} = g_e + 2\lambda/\Delta E_1; \quad g_{yy} = g_e + 2\lambda/\Delta E_2 \quad (6)$$

3. Charge trapping centres in TiO_2 . EPR results

As discussed in Section 1 charge carriers are trapped in the oxide matrix as a consequence of photochemical charge separation or, alternatively, of chemical treatments modifying the solid (e. g. annealing in vacuum, chemical reduction). A systematic knowledge of the features of trapped electron and holes is of vital importance to rationalize the behavior of the various polymorphs. We report here a systematic analysis of the EPR results obtained for trapped electrons and holes in TiO_2 polymorphs (essentially A and R). This is done in order to classify the diverse types of EPR signals (g values, lineshape etc.) and to establish a correspondence between the signal themselves and the variety of trapping sites.

3.1 Valence induction.

The method is well known to solid state chemistry and consists in the introduction, in regular positions of the solid network, of elements having extra electrons or an electron deficiency with respect to Ti and O. Excess electrons solids can be obtained both by cationic and anionic substitution. In the first case Nb or Sb ions have been used to substitute Ti while, in the second case, fluorine substitutes lattice oxygen. Alternatively, electron deficient systems can be obtained introducing Al in the crystals. In the case of polycrystalline TiO_2 the substitution is easily achieved using wet chemistry preparations of the solid such as the sol- gel technique or hydrothermal methods which easily lead to doped anatase. In the case of anatase the excess electrons are trapped under the form of Ti^{3+} centres which are visible in the EPR spectra. The two types of excess-electron solids (cation or anion substitution) can be written respectively as $Ti^{4+}_{(1-x)} Nb^{5+}_x Ti^{3+}_x O^{2-}_2$ and $Ti^{4+}_{(1-x)} Ti^{3+}_x O^{2-}_{(2-x)} F^-_x$. Niobium doping of polycrystalline anatase has been previously investigated by EPR by Kiwi et al.³⁸ and by Valigi et al.³⁹, while fluorine doping was reported by Halliburton (single crystals)⁴⁰ and by some of

us⁴¹. In the case of Al doping the solid can be written as $Ti^{4+}_{(1-x)} Al^{3+}_x O^{2-}_{2-x} (O^{2-h+})_x$ where a fraction of oxygen anions corresponding to the Al concentration localizes an hole (see below). Figure 2 reports the X band EPR spectra, recorded at 77K, of a Nb doped (2a) and of an Al doped (2b) materials. The former spectrum is similar to those obtained using Sb or F.

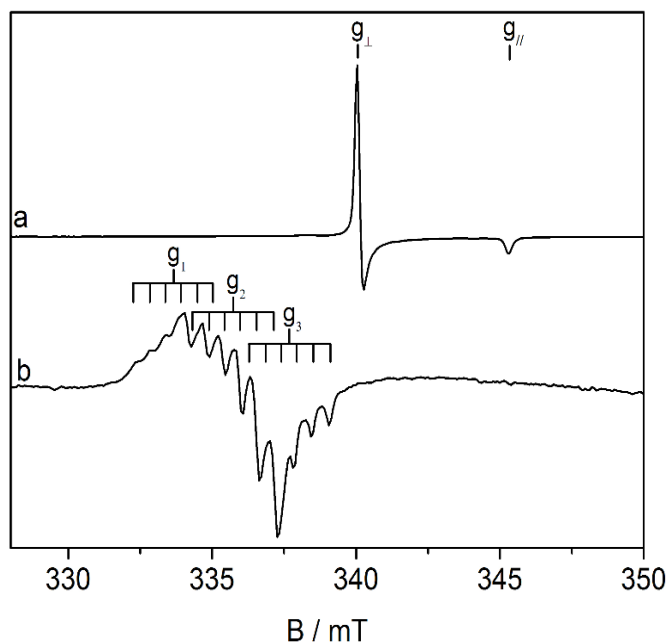


Figure 2. EPR spectra of a trapping electron centre (a) and a trapping hole ($Al-O^-$) centre in anatase.

The Ti^{3+} signal in Fig. 2a (hereafter signal A) is axial ($g_{zz} = g_{||} = 1.962$ and $g_{xx} = g_{yy} = g_{\perp} = 1.992$) and no break of this symmetry is observed even when the spectrum is recorded at much higher resolution (W band, 95GHz)⁴². As illustrated before this spectrum is the result of the compensation of the extracharge carried by the dopant. Recording the spectrum at increasing temperatures (Fig. 3) the line tends to broaden, the intensity to decline and eventually to disappears. Two are the possible causes of the described effect which are probably both operating in this case. The first one is the trend of the relaxation time values which, in several case of Ti^{3+} spectra, causes weakening of the intensity at temperatures higher than that of liquid nitrogen (77K). The second one is thermalisation of electrons from intra band gap states to the conduction band. To observe this effect around room temperature the intraband states must be, of course, very shallow (see Section 3). The paramagnetic centre corresponding to signal A constitutes the prototype of an electron-trapping site in bulk regular positions of the anatase lattice (thus not associated to oxygen vacancies). The same conclusions was reached by studies on photoinduced charge separation in irradiated TiO_2 systems kept in aqueous colloidal suspensions^{31, 43,44}.

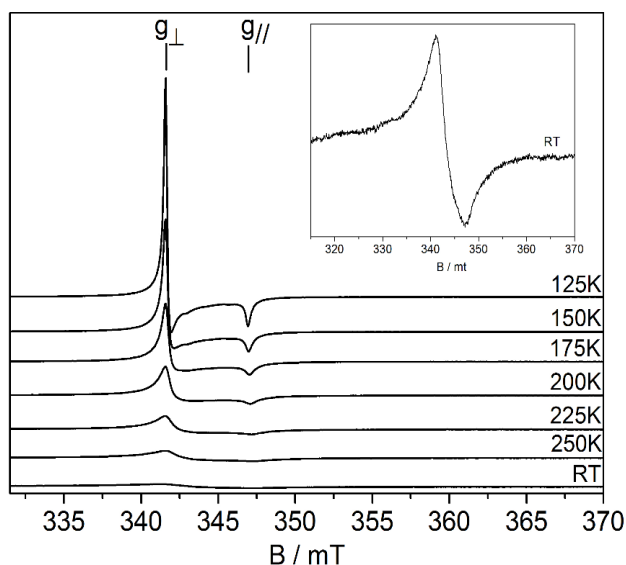


Figure 3. EPR spectra of Nb doped anatase in the temperature range 125K-RT. In the inset the spectrum at RT is reported with higher magnification.

Experiments in rutile with the same approach are not easily feasible. In fact if F-doped anatase is heated at high temperature to accomplish the anatase to rutile phase transition the sample loses completely the fluorine dopant. In the case of Nb doped titania it has been instead clear since the early studies of Chester⁴⁵ and Zimmermann⁴⁶ on single crystals that the excess electron resides on the dopant metal. In these papers the Authors observe at very low temperature the EPR spectrum of Nb⁴⁺ ions with the typical hyperfine structure of ⁹³Nb ($I=9/2$). In our powdered material the transformation of Nb doped anatase in rutile by high temperature treatment causes the modification of the EPR signal which moves at higher magnetic field at $g=1.981$ (as expected in the case of Nb⁴⁺) but the rich hyperfine structure remains unresolved at 77K (data not reported for brevity). To summarize, the valence induction in TiO₂ using excess electrons elements surprisingly leads to different results in the case of anatase and rutile. In the former case (F, Nb, Sb doping) the electron trapping sites are lattice titanium ions (and the axial signal A is the EPR fingerprint of such sites) while in the second case (Nb doped rutile) the electrons remain on the aliovalent dopant element.

The spectrum in Fig. 2b has been obtained in the case of Al³⁺ doped TiO₂ and is clearly due to an electron hole localized onto an O²⁻ ion proximity of an Al ion. The spectrum is rich of lines because of the hyperfine interaction with the $I=5/2$ ²⁷Al nucleus. The g values of the rhombic signal are $g_1=2.027$, $g_2=2.015$, $g_3=2.003$ and are typical of an O⁻ ion, which is the chemical manner to describe an electron hole localized on an oxide ion: (O²⁻h⁺). The hyperfine tensor of ²⁷Al is $A_1=0.5$ mT, $A_2=0.58$ mT, $A_3=0.61$ mT. The g values of the AlO⁻ hole centre are close to those of similar centres in other solids (SiO₂⁴⁷, ZrO₂⁴⁸). The reason of the hole localization

close to an Al^{3+} ion has to be searched in the small size of this cation which exert a strong electrostatic potential on the O^- ion.

3.2 Photoexcitation

The effects of UV irradiation of TiO_2 has been already described in several papers mainly concerning Anatase and P25. The seminal work in the field was performed by Graetzel and Howe³¹ on anatase and by the Thurnauer group mainly on the biphasic P25 system⁴³. In both cases the Authors irradiated at very low temperature colloidal aqueous suspensions (systems used in photocatalytic tests at RT). The presence of surface hydroxyls and water molecules favors in these case the stabilization of the carriers.

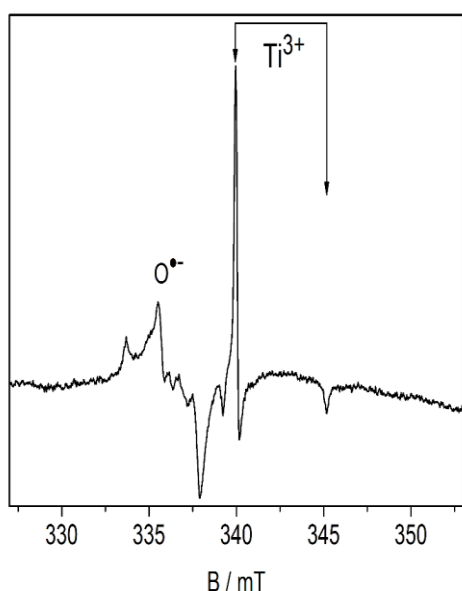


Figure 4. EPR spectra recorded at 77K of CVR anatase under UV irradiation. Spectrum recorded at 1 mW microwave power. The sample is irradiated under vacuum. Raising the temperature at RT the two carriers easily recombine.

Although in our experiments we also use polycrystalline materials, our approach is closer to that of surface science and of gas-solid interaction studies. We have thus irradiated fully dehydrated samples kept under vacuum obtaining anyhow evidence of charge separation and trapping (Fig.4).

Electrons, in these conditions, are also trapped on lattice titanium ions. The signal in Figure 4, in fact, is the same observed by valence induction (signal A with $g_{\parallel}=1.962$ and $g_{\perp}=1.992$). The trapped hole signal (O^-) is made up by the contribution of at least two akin species with similar but distinct parameters. At the microwave power employed to record the spectrum in Fig. 4 one of these species is dominant and has $g_1=2.027$, $g_2=2.015$, $g_3=2.003$. These values are similar but not exactly coincident with those previously

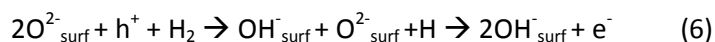
reported ^{25d} probably due to the fact that the spectrum in Fig. 4 is recorded under vacuum. The hole are trapped at the surface since they easily react with hole scavengers like molecular hydrogen.

3.3 Electron injection

Electron injection in the solid through the surface can be easily achieved exposing a sample to atomic hydrogen. This can be generated either by microwave discharge in H₂ with direct formation of H atoms over the solid or by UV irradiation in H₂ atmosphere. In the first case the H atom ionizes injecting an electron in the solid^{49, 50}:



In the second case the UV light induces charge separation with formation of an electron and a hole. The surface migrated hole reacts with molecular hydrogen to give an hydroxyl group and an H atom:



In both experiments the reducing agent is atomic hydrogen and the results, in term of EPR spectra, are identical. Figure 5 reports two EPR spectra, in a restricted magnetic field range, related to an hydrogen treated and a deuterium treated anatase respectively. The two spectra are practically superimposable indicating that there is no appreciable interaction of the unpaired electron with the parent H (D) nucleus.

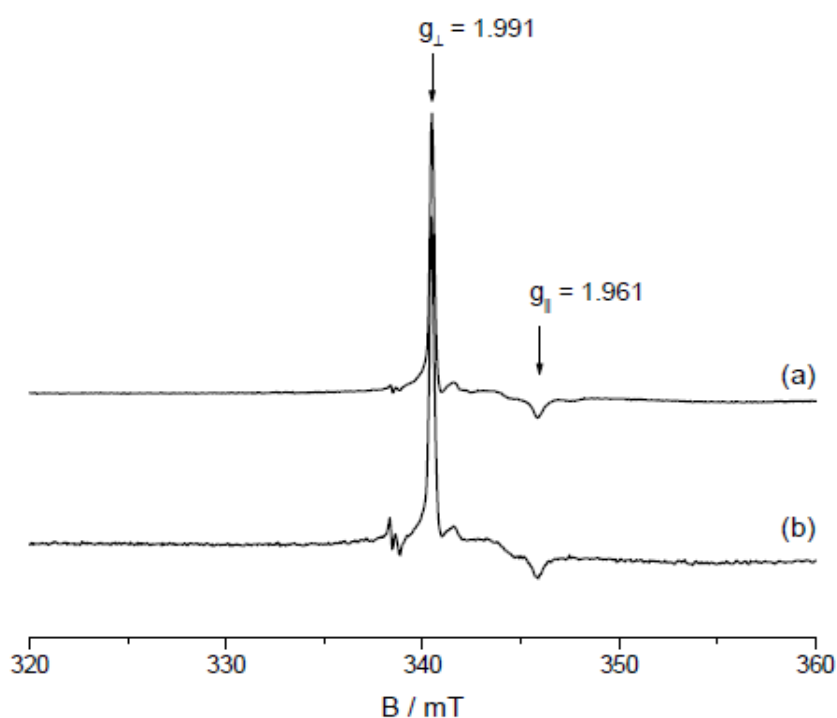


Fig. 5 EPR spectra of CVR anatase contacted with atomic hydrogen (a) and deuterium (b)

They are dominated by the previously discussed signal A which is however perturbed by the onset of a second broad signal. This second signal is better detected by the Electron Spin Echo (ESE) detected EPR experiments (Fig.6).

The ESE detected EPR spectrum corresponds to the absorption of the conventional CW-EPR spectrum and is more effective in the detection when, as in the present case, broad signals are present which are hardly observed in the CW derivative spectrum. The spectra of H treated TiO₂ (Fig. 5 and 6) are thus more complex than those in Fig. 2a and 3 as they include two distinct signals. The broad unstructured signal (signal B) is centered at approximately $g = 1.93$ and extends over approximately 35 mT. This means that, despite what appears in Fig. 5, the number of paramagnetic centres corresponding to signal B is much higher than that corresponding to signal A.

The most likely source of broadening, determining the large linewidth of signal B, has been ascribed⁴² to strain effects associated to the presence of different sites with slightly different local environment and therefore slightly different EPR parameters. This situation is indeed occurring at the surface of anatase nanocrystals which is made up by different faces each of them exposing ions having at least two different coordinations. The presence of morphological defects of the crystals like edges, steps or kinks further complicate the picture. The surface nature of Ti³⁺ ions corresponding to signal B has been confirmed by an ad hoc ESEEM, (Electron Spin Echo Envelope Modulation) experiments on anatase nanocrystals enriched at the surface with ¹⁷O.

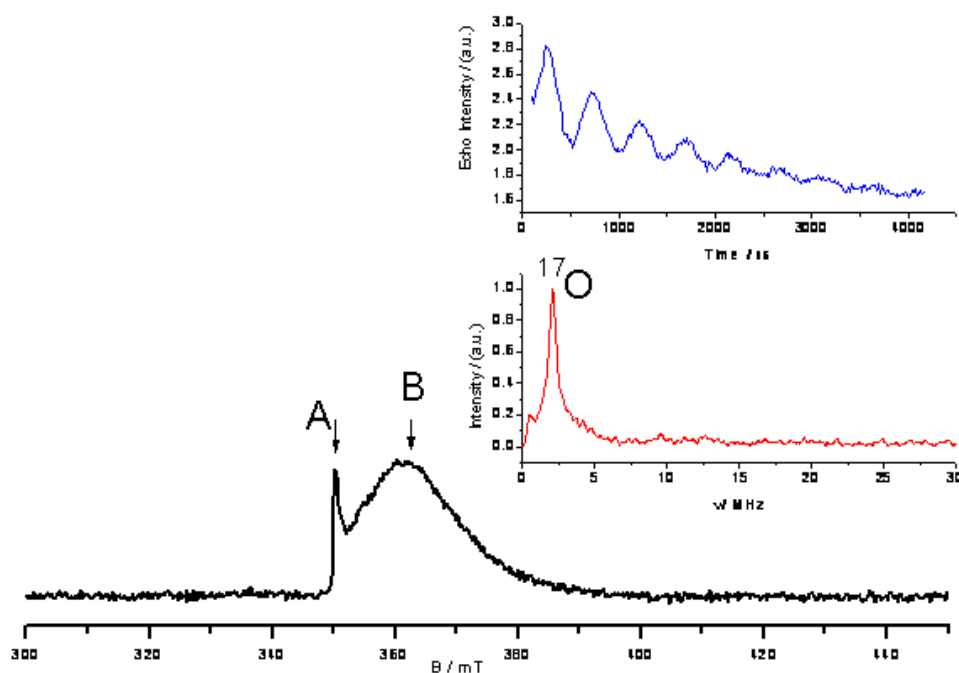


Fig.6. ESE detected (T=10K) EPR spectrum of ¹⁷O enriched anatase treated with atomic H. In the inset the 3 pulse ESEEM spectrum taken at observer position B and the corresponding frequency domain spectrum.

The local enrichment has been obtained by annealing at 773K the solid (oxygen depletion) and then restoring the oxygen content by reoxidation in $^{17}\text{O}_2$. In this way the surface region, more affected by oxygen depletion, becomes isotopically enriched. The three-pulse ESEEM pattern⁴² shows an ^{17}O modulation depth which is rather strong in the case of species B (inset of Fig. 6), indicating a high number of ^{17}O nuclei interacting with the Ti^{3+} centres, and nearly absent in the case of species A (not reported). This can only be explained, as the ^{17}O enrichment is limited to the surface and subsurface region of the sample, in terms of the surface nature of the species corresponding to signal B. The same conclusion on the nature of the broad signal at $g=1.93$ was proposed by Thurnauer and co-workers^{43,51} on the basis of its behaviour upon reactivity of the solid. Summarizing, the electron injection from an external source (H) leads to two types of electron trapping. A minority of the trapped electrons stabilize on subsurface or bulk Ti^{4+} electron traps (signal A) while the majority (B) is stabilized onto variously coordinated trapping electron ions at the solid surface.

3.4 Reductive annealing of the solid.

The propensity of TiO_2 to loose oxygen by annealing under vacuo transforming from an insulator to a n-type semiconducting oxide has been described in the Introduction (eq. 1). Oxygen depletion generates, beside oxygen vacancies, excess electrons which are trapped in the solid. Fig. 7 describes in terms of EPR the effect of a progressive reduction of Anatase by sequential annealing steps (15 min each) from 470K to 770K.

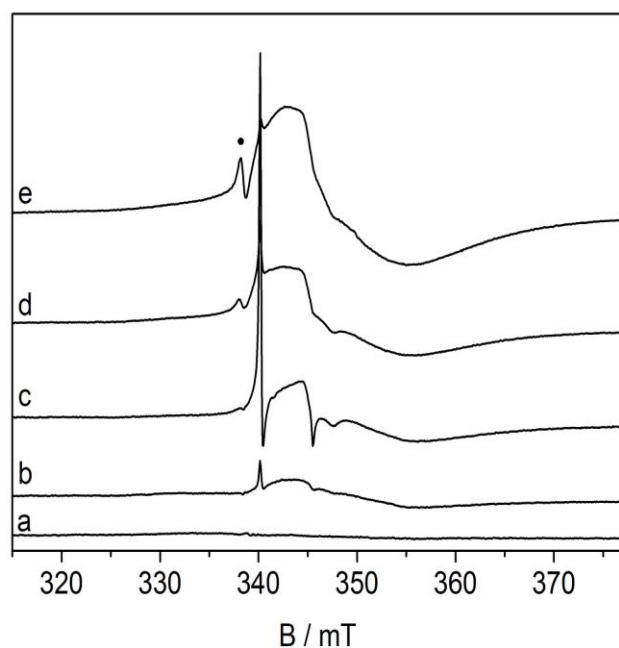


Fig. 7. Thermal annealing in dynamic vacuum of sol-gel prepared anatase at increasing temperature adopting 15' steps. (a) starting material, (b) 470 K, (c) 570 K, (d) 670K, (e) 770K.

The figure shows that, in the early stages of the reduction, the bulk Ti^{3+} species (species A) is clearly visible in the spectrum and its intensity grows till the annealing step at 573K. In the following steps of the treatment the signal of species A tends to overlap with the broad and featureless line of signal B, the surface titanium reduced species at $g= 1.93$ already described in Section 3.3. Eventually signal B becomes dominant in the EPR spectrum and the disordered, defect-rich phase corresponding to this signal expands to encompass the subsurface region where species A was initially present. In such a condition the anatase sample is colored (pale grey-blue) and EPR spectra recording becomes difficult due to the presence of conduction electrons in the material.

3.5 Electron trapping centres in rutile.

In the case of rutile the surface treatment described in Sections 3.3 and 3.4 leads to signals which often tend to become broad and featureless particularly in the case of extremely small crystals. This has originated some confusion in the literature. To determine exactly the typical parameters of excess electrons in rutile it is necessary to explore the early stages of electron injection as done in the experiments reported in Fig. 8 where two EPR spectra obtained by gentle annealing of microcrystalline rutile (Fig. 8a and b) are compared. Strictly similar spectra are obtained by reaction with H atoms. Both spectra in Fig. 8 are due to Ti^{3+} centers. The first one (8a) shows up after a short annealing at 373K while the second (8b) appears after a similar treatment at 673K. The two signals are basically the same except for the linewidth which is larger in the second spectrum, as shown by computer simulation. The signal in Fig 8a due to its low intensity is fully resolved and has orthorhombic g tensor with $g_1 = 1.969$, $g_2 = 1.960$ and $g_3 = 1.949$. It is absolutely reasonable to consider these parameters as prototypical for the regular lattice titanium site (hereafter C) trapping an electron (Ti^{3+}). Differently from the case of anatase (Fig.6 and 7) no signal at different g arises for prolonged annealing, the only result being a progressive broadening of the original signal which eventually become featureless. It does not exist therefore a distinct EPR signal for surface electron traps on rutile.

The question of the presence in reduced rutile (and in general in titanium dioxide) of significant amounts of ions located in interstitial sites has been widely discussed in the literature in particular when considering ion migration during reoxidation of surfaces reduced by sputtering⁵² which occurs via diffusion of bulk cations occurring also through interstitial positions. Apart from this evidence which concerns a dynamic phenomenon, evidence of the presence of stable interstitial Ti^{3+} centres in reduced rutile was obtained by EPR for a series of single crystals⁵³ and in the case a single crystal rod, studied by Aono and Hasiguti, heated in a preevacuated capsule in the range 1300-1700K⁵⁴. In the second case only, the Authors were able to

derive the exact orientation of the observed Ti^{3+} species in the crystal (firmly proving the interstitial nature of the center) and provided the principal elements of its g tensor ($g_1 = 1.9780$, $g_2 = 1.9746$ and $g_3 = 1.9414$)⁵⁴. In the case of polycrystalline materials and differently from anatase, the rutile polymorph can be directly prepared in sub stoichiometric form. Colored blue TiO_2 materials are quite deeply reduced but are stable in air. Due to their visible light absorption properties, such materials have been seldom used in experiments of photocatalysis under visible light⁵⁵. We have directly prepared reduced rutile by hydrolysis of $TiCl_4$ with a stoichiometric amount of water under N_2 flow. The powder was kept under N_2 flow for 2 hours and successively heated up to 973 K for 10 minutes under N_2 flow. The final product was a blue TiO_2 powder mostly in the Rutile form. The sample shows an EPR signal at 4K which is reported in Fig. 8 c and 8d. In the second case the spectrum is the first derivative of an Electron Spin Echo (ESE) detected spectrum which is well resolved and allows an accurate measure (see computer simulation) of the g tensor elements which are⁵⁶ $g_1 = 1.9787$, $g_2 = 1.9750$ and $g_3 = 1.9424$, compatible with a tetragonally distorted octahedral symmetry of the centre further reduced by an intrinsic local asymmetry of the Ti coordination (*vide infra*).

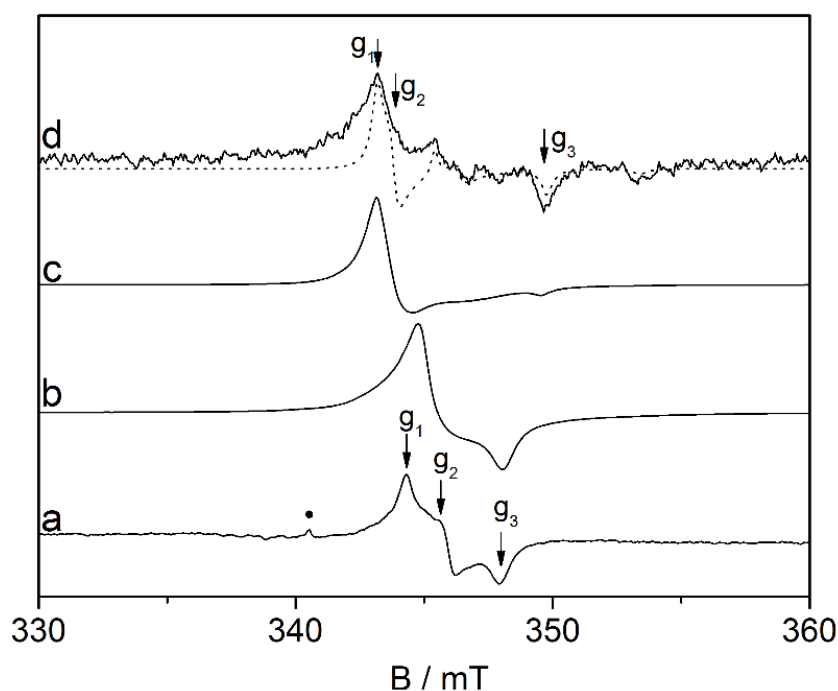


Fig. 8. EPR spectra recorded at 77K of microrutile annealed under vacuum at 373K (a) and at 673 for 15 min (b). The dot in (a) indicates a trace of Ti^{3+} ions in anatase (signal A). EPR spectra at 4K of the as prepared “blue” rutile sample prepared via hydrolysis of $TiCl_4$ and observed by CW-EPR(c) and ESE-detected EPR (d) .

This set of parameters of the rhombic signal observed in polycrystalline blue rutile (Fig. 8 c and d) nearly exactly coincide with those recorded in the mentioned single crystal study⁵⁴. On the basis of the close similarity of the two sets of parameters, the signals in Fig. 8c and 8d (signal D) must be considered the powder EPR spectrum of interstitial Ti^{3+} ions in rutile. The distinction between regular lattice sites and interstitial site in rutile is very delicate as the g values of the signals (Figure 8) are quite close one to the

other but unambiguously distinct. This is not very surprising if one consider the coordination of titanium ions in the two sites (lattice and interstitial) which are extremely similar. A scrutiny of the rutile structure⁵⁷ indicates, in fact, that the coordination of titanium ions in lattice position and in interstitial position of this structure mainly differ in the orientation of the fourfold axis since in both cases one has an octahedrally distorted environment of oxygen spheres. This is not the case of anatase where an interstitial site has a quasi pyramidal symmetry quite lower than that of the regular site⁵⁸.

The g values of the main electron trapping sites present in the two main polymorphs of TiO₂ are resumed in Table 2 together with the conditions of their formation.

Signal	Polymorph	Trapping site	g values			Notes
A	Anatase	Regular lattice site	$g_{\perp}=1.992$	$g_{ }=1.962$		Narrow (Fig.1). Formed by: i) valence induction, ii) photoecitation, iii) electron injection, iv) reductive annealing
B		Surface sites (disordered environment)	$g_{av} = 1.93$			Broad because of site heterogeneity (Fig.4) Formed by i) electron injection, ii) reductive annealing
C	Rutile	Regular lattice site	1.969	1.960	1.949	Formed by: i) electron injection, ii) gentle reductive annealing
D		Interstitial site	1.9787	1.9750	1.9424	Formed by: i) substoichiometric preparation ii) extreme reductive conditions ⁵²

Table 2. g values of various electron trapping centers in anatase and rutile.

The evident asymmetry observed in Table 2 and related to the lack of signals due to both surface Ti³⁺ in rutile and interstitial Ti³⁺ in anatase, has been partially commented before in this Section. We can add here that the presence of interstitial Ti³⁺ in anatase (which is unlikely due to the strong asymmetry of the site discussed just above) can not be however completely excluded. The signals of these sites (if any) may be buried in the broad signal B whose width implies a strong heterogeneity. More difficult to comment on the absence of a specific signal for Ti³⁺ at the surface of rutile. This could be due to a possible lower stability of surface ions with respect to bulk ones with consequent migration of the excess electrons towards the inner sites of the solid. However, there is still insufficient evidence for a conclusive clarification of this issue.

3. Electron localization in trapping centres .

As mentioned in the introduction the space distribution of the trapped electron wave function is critical for all applications of TiO_2 implying generation, stabilisation and dynamics of charge carriers. This question is still debated and opposite conclusions (electron localized on a single titanium ion or delocalized on several ions in a relatively large volume) are often derived by various experimental approaches^{32,33}. Furthermore, the theoretical descriptions of reduced titanium oxide do not contribute to solve the dilemma since, as recently shown, it happens that fully localized and highly delocalized solutions show similar energy values limiting the possibility of a clear indication derived from theory²¹. As far as EPR is concerned, the spin density distribution, which is a strong point of the technique, cannot be derived in the case of Ti^{3+} ions since the g factor only is available. The absence in the system of magnetic nuclei (nuclear spin $I \neq 0$) in sufficient concentration, in fact, prevents the measurement of the electron-nucleus interaction (hyperfine interaction) which is the parameter providing information on the spin density distribution. To start overcoming this problem and considering that the direct insertion in the solid of Ti magnetic nuclei (^{47}Ti and ^{49}Ti) is not an easy task, our group has proposed a method based on the inclusion by chemical methods of ^{17}O ($I=5/2$) into the oxide lattice. This method, successfully adopted in the case of alkali earth oxides⁵⁹ which have the same problem of isotopic composition found in TiO_2 , allows the measure of the so called superhyperfine interaction. This interaction, in principle, allows to measure the electron spin density localized onto the ligands of a coordination compound having a paramagnetic metal centre. In our case we intended to evaluate the spin density on the oxygen atoms surrounding Ti^{3+} in TiO_2 . To obtain ^{17}O bulk-enriched TiO_2 i.e. various preparations of the oxide by hydrolysis of TiCl_4 employing ^{17}O enriched water were performed. We thus obtained in this way bare anatase, F-doped anatase and blue reduced rutile (Section 3.5). Fully oxidized rutile was obtained by anatase transformation. The typical CW-EPR spectra of Ti^{3+} in anatase and rutile shown before in this paper do not change after ^{17}O enrichment indicating that the expected superhyperfine interactions are too small to be detected by this technique. Therefore, in order to probe the spatial extent of the unpaired electron wave function for these Ti^{3+} interstitial ions, Hyperfine Sublevel Correlation spectra have been recorded at different field positions corresponding the principal g values of the dominant EPR signals on two different samples namely F doped anatase (bulk lattice site, Table 2 species A) and substoichiometric rutile (interstitial site; Table, 2 species D). Typical HYSORE spectra are reported in Figure 9 and show the presence of different ^{17}O correlation peaks in both (+,+) and (-,+) quadrants, which are absent in the non enriched samples. The most striking difference between the two samples is in the strong hyperfine region (-,+ quadrant, left hand side of the figure). In the case of substoichiometric rutile in fact two off diagonal cross peaks at about (-2,6) MHz and (-6,2) MHz in the (-,+) quadrant are present, which are separated by approximately $2\nu_{\text{O}}$ ($\nu_{\text{O}} = 2.021$ MHz) and relate the ^{17}O $m_{\frac{1}{2}} \rightarrow -\frac{1}{2}$ transitions of the two m_s manifolds. Computer simulation analysis of spectra recorded at various magnetic field positions allowed to extract the full ^{17}O hyperfine tensor.⁵⁶ From these values a Fermi

contact (a_{iso}) term of about 8 MHz and an anisotropic coupling $2T \approx 2$ MHz was derived (Table 3). The origin of this (negative) Fermi contact term can be understood considering the nature of the chemical bond between the Ti ions and the oxide ligands. The bonding interaction in TiO_2 is characterized by a π overlap between the metal d and oxygen p orbitals⁶⁰ This interaction when paramagnetic Ti^{3+} ions are present, will induce in a negative spin density on the oxygen as a result of a spin polarization mechanism, the positive sign of a_{iso} being due to the negative ^{17}O nuclear g factor ($g_n = -0.757516$). This fairly large (positive) ^{17}O hyperfine constant appears to be indeed a distinctive feature of d^1 metal-oxygen bonding mechanisms as observed in some esquo molecular cations where metal-oxygen bonds are based on π overlap interactions⁶¹. Based on the similarities between the nature of the chemical bond between solid TiO_2 and d^1 molecular complexes we have, in fact, investigated in detail the molecular $[\text{Ti}(\text{H}_2^{17}\text{O})_6]^{3+}$ esquo complex⁶², which is a typical example of non delocalized system. Remarkably we observed in this case a ^{17}O Fermi contact term of the same order (≈ 8 MHz) which strongly suggests that excess electrons in the blue rutile sample are (at 4 K) largely localized over a single Ti ion, which bears strong similarities to a genuine Ti^{3+} molecular cation.

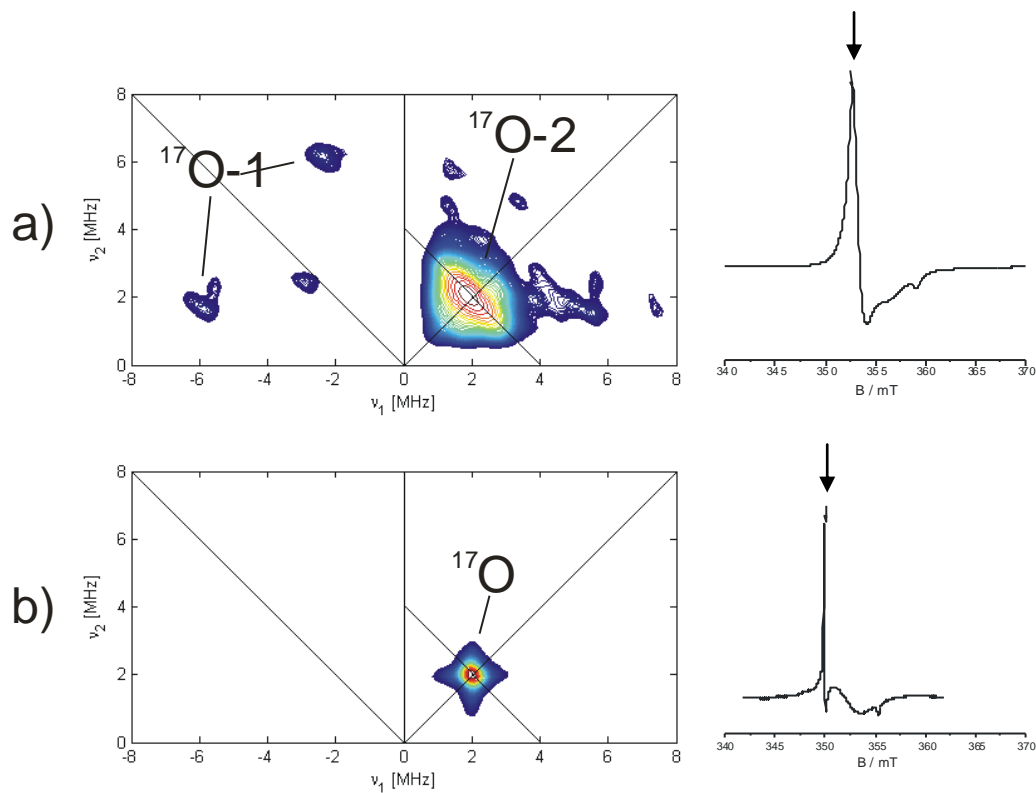


Figure 9. ^{17}O HYSCORE spectra of a) interstitial Ti^{3+} ions in rutile and b) Ti^{3+} ions in F doped anatase. The corresponding CW EPR spectra are shown on the right hand side of the Figure. HYSCORE spectra were recorded at 4K

with $\tau=120$ ns. The observer position corresponds in both case to the perpendicular component of EPR spectrum and is indicated by an arrow in the EPR spectra.

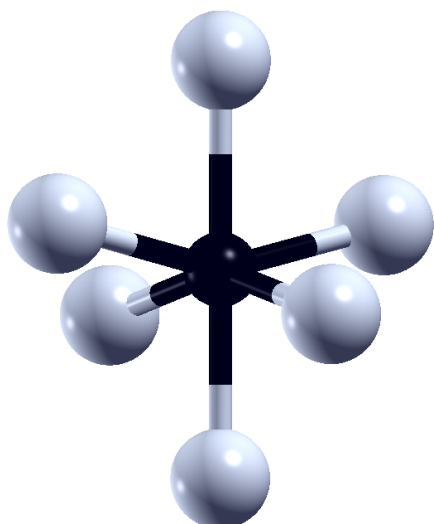
A totally different scenario is present in the case of anatase (Fig 9b). No traces of ^{17}O correlation peaks could be found in the (-,+) quadrant of HYSORE spectra. The only signal observed was a peak centered at the ^{17}O nuclear Larmor frequency, in the (+,+) quadrant with maximum extension of about 2 MHz. This clearly indicates the sole presence of weakly coupled ^{17}O .

System	g tensor			^{17}O A tensor/MHz				Reference
	g_1	g_2	g_3	a_{iso}	A_1	A_2	A_3	
Esaquo Ti^{3+}	1.994	1.896	1.896	7.5	-0.5	2.0	-1.5	62
Interstitial Ti^{3+} in rutile single crystal	1.9780	1.9746	1.9414	-	-	-	-	54
Ti^{3+} in ^{17}O rich reduced rutile (sign. D)	1.9787	1.9750	1.9424	8	-2.5	0.5	2.0	56
Ti^{3+} in anatase lattice sites (sign. A)	1.9920	1.9920	1.960	<0.2	und.	und.	und.	42

Table 3. Comparison of the g and ^{17}O hyperfine parameters concerning the Ti^{3+} species discussed in this paper.

The absence of a distinct ^{17}O coupling in the case of trapping electron centers in anatase is therefore strongly symptomatic of an unpaired electron wave functions sampling a larger number of oxide anions and thus indicating a delocalized nature of the defect with drop of the hyperfine interaction to values under the detection limit of the HYSORE technique. There are three other important elements, beside the described observation, which suggest that a certain degree of delocalization of the Ti^{3+} wavefunction in anatase is the correct physical description for this system. These elements can be discussed as follows:

a. A delocalized solution is not excluded by theory. The nature of the electron trapped states in Titania has been recently tackled by Di Valentin et al.²¹ who found two opposite solutions (excess electron fully localized in a d_{xy} orbital and electron delocalized over all the d_{xy} orbitals of the supercell used for the calculations) having the same total energy. In the former case Ti^{3+} is an intra band gap state about 0.8 eV (ca.1550nm, NIR region) below the bottom of the conduction band while the delocalized state lies at the bottom of the conduction band itself. By the way in our optical investigation of n-type doped anatase (Nb or F doped) we never found evidence of NIR absorption.



Scheme 3. The local symmetry of Ti ions in anatase.

b. The nature of signal A must be considered again in the perspective of the electron localisation problem. Signal A (Fig. 2, Table 1) has an axial structure fully confirmed even in the high resolution conditions of EPR recorded in W band (EPR 90GHz). The axial nature of the g tensor is not compatible with the local symmetry of Ti^{4+} ions in unperturbed bulk anatase (Scheme 3) which shows quite strong distortions in the equatorial plane and the absence of fourfold (or threefold) axes required to ensure the axial symmetry of g . In other words, an hypothetical molecular compound of Ti^{3+} with the symmetry shown in Scheme 3 could not have an axial g tensor. One could infer that the localization of an extra-electron most likely induces polarisation of the original trapping site, however an increase of its symmetry upon trapping, leading to an axial situation, seems rather unlikely. It is not surprising in fact that in the case of rutile electron trapping in sites having geometry quite similar to that shown for anatase generates in all cases rhombic signals (Table 1, signals C and D). The nature of signal A therefore, in agreement with HYSCORE results, most probably corresponds to an electron delocalization over a discrete number of lattice sites with a wavefunction maintaining the typical axial symmetry clearly indicated by the g tensor.

c. The different behaviour of anatase and rutile in term of electron conduction properties are known in the literature. In a careful comparison of conductivities and Hall effect of rutile and anatase single crystal films annealed under vacuum at 673K and 723K, H. Tang et al.⁶³ individuated a marked difference in the behavior of the two polymorphs. The reduced rutile resistivity decreases with decreasing temperature and conduction is ensured either by thermal excitation in CB (at high temperature) or by hopping from donor (Ti^{3+}) centers. The donor state radius is evaluated, in this case, of the order of 2.6\AA . Conductivity of partially reduced anatase is of metallic type and nearly constant with temperature. In such conditions, and differently from rutile, the Hubbard gap in the donor bands vanishes. The effective mass of the carrier is small and the Bohr radius of the donor state is around 15\AA significantly exceeding the interionic distance. A further element of difference is given by the position, in the two cases, of the energy levels of excess

electron centres (Ti^{3+}). In the case of rutile (interstitial sites, coloured material) these ions correspond to localized states well below the conduction band. In the case of anatase, when the only signal A is present (Fig.2a), the material does not show absorption in the visible (see point a in this Section) and the Ti^{3+} should resonate with the conduction band, in agreement with the proposed model of electron delocalisation.

These data establish a clear-cut separation of the behavior of anatase and rutile and seem in agreement with our data on electron localization in the two polymorphs.

CONCLUSIONS

In the present paper we have attempted to rationalize, using the Electron Paramagnetic Resonance approach, the problem of electron trapping in titanium dioxide polymorphs individuating, without ambiguity, the EPR signals corresponding to well defined trap sites in both anatase and rutile. The signals are characterised in terms of the only g tensor values because of the lack of magnetic nuclei producing hyperfine structures. The electron trapping Ti^{3+} centers have been obtained using different procedures (photoexcitation, valence induction, surface reactivity and, as often done in surface science studies, thermal annealing in vacuo). At variance of what generally thought, a series of independent and well defined EPR signals can be found in all cases examined with the only exception of the surface Ti^{3+} centres in Anatase which, though being characterised by a definite g value at 1.93, display a very broad and substantially featureless signal due to site heterogeneity. In the other cases (bulk centers in anatase and in rutile, interstitial centres in rutile) we have provided (Table 2) a guideline to individuate the features of each centre. As to the interstitial form of Ti^{3+} in rutile it has been shown that it forms in particularly non stoichiometric reduced systems (blue rutile) while softer reducing methods tend to cause electron trapping in regular lattice sites. The question of the degree of localisation of the electrons in the trap is at the centre of a lively debate. In a recent paper by Krüger et al., performed using Resonant Photoelectron Diffraction³² the question was raised in these terms: *“There is however no experimental answer to the question on which Ti sites the excess electrons are localized and this is because there has been, to date, no suggestion of any relevant experimental approach to unravel charge localization.”* We have contributed to the debate using an experimental approach based on hyperfine EPR techniques (namely HYSORE) coupled to ¹⁷O isotopic substitution obtained via specific synthesis. In this way we have evidenced a net difference in the two cases which was possible to explore (interstitial rutile and bulk anatase). In the former case (Table 3) the spin density on the six oxygens surrounding the Ti centre is that typical of a true molecular cation with the unpaired electron largely localized over a single Ti ion. As opposite in the case of anatase lattice centres the spin density onto the oxygen ions is much lower suggesting a high degree of delocalisation of the excess electron wave function. These findings, which could find further and conclusive confirmation if

materials enriched with ^{47}Ti and ^{49}Ti isotopes would be available, represent a contribution to the scientific debate on titanium dioxide and in particular on some unresolved problems such as that concerning the different photochemical and photocatalytic properties of the two main polymorphs.

ACKNOWLEDGMENTS

This work has been supported by the Italian Ministry of University and Research, MIUR through the funds "Programs of National Relevance" (PRIN-2009) and the "National Funding for Basic Research" with a project entitled "Oxides at the nanoscale: functionalities and applications" (FIRB 2011, RBAP115AYN). We also wish to acknowledge the support of the COST Action CM1104, "Reducible oxides, chemistry, structure and functions".

REFERENCES

- 1 K. Honda and A. Fujishima *Nature*, 1972, **238**, 37.
- 2 A. L. Linsebigler, G. Q. Lu and J. T. Yates, *Chem. Rev.*, 1995, **95**, 735.
- 3 A. Fujishima, T. N. Rao and D. A. Tryk, *J. Photochem. Photobiol. C*, 2000, **1**, 1.
- 4 Photocatalysis: Fundamentals and Applications; N. Serpone, E. Pelizzetti Eds; Wiley & Sons: Chichester, 1989
- 5 A. Fujishima, X. Zhang and D.A. Tryk, *Surf. Sci. Rep.*, 2008, **63**, 515.
- 6 M. Cho, H. Chung, W. Choi and J. Yoon, *Water Research*, 2004, **38**, 1069.
- 7 M. Nozawa, K. Tanigawa, M. Hosomi, T. Chikusa and E. Kawada, *Water Science and Technology*, 2001, **44**, 127.
- 8 T. Watanabe, A. Nakajima, R. Wang, M. Minabe, S. Koizumi, A. Fujishima and K. Hashimoto, *Thin Solid Films*, 1999, **351**, 260.
- 9 A. Hagfeldt and M. Grätzel, *Chem. Rev.*, 1995, **95**, 49.
- 10 X. Chen and S. S. Mao, *Chem Rev.*, 2007, **107**, 288.
- 11 M. Chiesa, C. Paganini and E. Giamello, *Appl. Mag. Res.*, 2010, **37**, 605.
- 12 U. Diebold, *Surf. Sci. Rep.* 2003, **48**, 53-229.
- 13 T. L. Thompson and J. T. Yates, *Chem. Rev.*, 2006, **106**, 442.
- 14 M. A. Henderson, *Surf. Sci. Rep.*, 2011, **66**, 18.
- 15 P.W. Tasker, *J. Phys. C*, 1979, **12**, 4977.
- 16 J. P. La Femina, *Crit. Rev. Surf. Chem.*, 1994, **3**, 297.
- 17 a) N. A. Deskins and M. Dupuis, *J. Phys. Chem. C*, 2009, **113**, 346-358; b) N. A. Deskins, R. Rousseau and M. Dupuis, *J. Phys. Chem. C*, 2010, **114**, 5891.
- 18 a) Z. Lin, A. Orlov, R. M. Lambert and M. C. Payne, *J. Phys. Chem. B*, 2005, **109**, 20948; b) C. Di Valentin, G. Pacchioni and A. Selloni, *Phys. Rev. Lett.*, 2006, **97**, 166803; c) E. Finazzi, C Di Valentin and G. Pacchioni, *J. Phys. Chem. C*, 2009, **113**, 3382; d) S. Cretién and H. Metiu, *J. Phys. Chem. C*, 2011, **115**, 4696.
- 19 G. Li, N. Dimitrijevic, L. Chen, G. Nichols, T. Rajh and K. A. Gray, *J. Am. Chem. Soc.*, 2008, **130**, 5402.
- 20 V. N. Kuznetsov and N. Serpone *J. Phys. Chem. C*, 2009, **113**, 15110.
- 21 C. Di Valentin, G. Pacchioni and A. Selloni, *J. Phys. Chem. C*, 2009, **113**, 20543.
- 22 M. A. Henderson, W.S. Epling, C.H. F. Peden and C. L. Perkins, *J. Phys. Chem. B*, 2003, **107**, 534.
- 23 V. M. Komenko, K. Langer, H. Rager and A. Fett, *Phys. Chem. Miner.*, 1998, **25**, 338.
- 24 R.L. Kurtz, R. Stock-Bauer and T. E. Madey, *Surf. Sci.*, 1989, **218**, 178.
- 25 a) R. D. Iyengar, M. Codell, J. S. Karra and J. Turkevich, *J. Am. Chem. Soc.*, 1966, **88**, 5055; b) P. Meriaudeau, M. Che and C.K. Jørgensen, *Chem. Phys. Lett.*, 1970, **5**, 1313; c) M. Aono and R. R. Hasiguti, *Phys. Rev. B*, 1993, **48**, 12406; d) O. I. Micic, Y. N. Zhang, K. R. Cromack, A. D. Trifunac and M.C. Thurnauer, *J. Phys. Chem. B*, 1993, **97**, 7277; e) J. M. Coronado, A. J. Maira, J. C. Conesa, K. L. Yeung, V. Augugliaro and J. Soria, *Langmuir*, 2001, **17**, 5368; f) M. Li, W. Hebenstreit, U. Diebold, A. M. Tyryshkin, M. K. Bowman, G. G. Dunham and M. A. Henderson, *J. Phys. Chem. B*, 2000, **104**, 4944; g) A.L. Attwood, D.M. Murphy, J. L. Edwards, T.A. Egerton and R.W. Harrison, *Res. Chem. Intermediates*, 2003, **29**, 449; h) T. Berger, M. Sterrer, O. Diwald, E. Knozinger, *J. Phys. Chem. B*, 2005, **109**, 6061; i) D.C. Hurum and K. A. Gray, *J. Phys. Chem. B*, 2005, **109**, 977.
- 26 M. Chiesa and E Giamello "Electron Paramagnetic Resonance of Charge Carriers in Solids" in M. Brustolon and E. Giamello Ed.s *Electron Paramagnetic Resonance: a practitioner's toolkit* Wiley 2010.
- 27 M. Chiesa, E Giamello and M. Che, *Chem. Rev.*, 2010, **110**, 1320.
- 28 P.H. Zimmerman, *Phys Rev B*, 1973, **8**, 3917.
- 29 S. Yang, L.E. Halliburton, A. Manivannan, P. H. Bunton, D. B. Baker, M. Kemm, S. Horn and A. Fujishima, *Appl. Phys. Lett.*, 94, **2009**, 162114.

- 30 S. Yang and L. E. Halliburton, *Phys Rev. B*, 2010, **81**, 035204.
- 31 a) R. Howe and M. Gratzel, *J. Phys. Chem.*, 1985, **89** 4495.; b) R.F. Howe and M. Gratzel, *J. Phys. Chem.* 1987, **91**, 3906.
- 32 P. Krüger, S. Bourgeois, B. Domenichini, H. Magnan, D. Chandresris, P. Le Fevre, A. M. Flank, J. Jupille, L. Floreano, A. Cossaro, A. Verdini and A. Morgante, *Phys. Rev. Lett.*, 2008, **100**, 055501.
- 33 S. Wendt, P. T. Sprunger, E. Lira, G. K. H. M. Madsen, Z. Li, J. Hansen, J. Matthiensen, A. Blekinge-Rasmussen, E. Lægsgaard, B. Hammer and F. Besenbacher, *Science*, 2008, **320**, 1755.
- 34 a) C. Di Valentin, G. Pacchioni, A. Selloni, S. Livraghi and E. Giamello, *J. Phys. Chem. B*, 2005, **109**, 11414; b) S. Livraghi, M.C. Paganini, E. Giamello, A. Selloni, C. Di Valentin and G. Pacchioni, *J. Am. Chem. Soc.*, 2006, **128**, 15666; c) S. Livraghi, M.R. Chierotti, E. Giamello, G. Magnacca, M.C. Paganini, G. Cappelletti and C.L. Bianchi, *J. Phys. Chem. C*, 2008, **112**, 17244; d) F. Napoli, M. Chiesa, S. Livraghi, E. Giamello, S. Agnoli, G. Granozzi, G. Pacchioni and C. Di Valentin, *Chem. Phys. Lett.*, 2009, **477**, 135. e) G. Barolo, S. Livraghi, M. Chiesa, M.C. Paganini, E. Giamello, *J. Phys. Chem. C*, 2012, **116**, 20887.
- 35 Electron Paramagnetic Resonance. A Practitioner's toolkit, M. Brustolon, E. Giamello Eds. (2009) Wiley, Hoboken (USA)
- 36 P. Pietrzyk, Z. Sojka, E. Giamello, Electron Paramagnetic Resonance Spectroscopy in: M. Che and J. Vadrine Eds, *Characterisation of Solid Materials and Heterogeneous Catalysts*. 2012 Wiley VCH verlag GmbH&Co. KGaA. 343-406
- 37 M. Chiesa, E. Giamello, C. Di Valentin and G. Pacchioni, *Chem. Phys. Lett.*, 2005, **403**, 124.
- 38 J. Kiwi, J. T. Suss and S. Zsapiro, *Chem. Phys. Lett.*, 1984, **106**, 135.
- 39 M. Valigi, D. Cordischi, G. Minelli, P. Natale, P. Porta and C.P. Kreijzers, *J. Solid State Chem.*, 1988, **77**, 255.
- 40 S. Yang and L. E. Halliburton, *Phys. Rev. B*, 2010, **81**, 035204.
- 41 A. M. Czoska, S. Livraghi, M. Chiesa, E. Giamello, E. Finazzi, C. Di Valentin, G. Pacchioni, S. Agnoli and G. Granozzi, *J. Phys. Chem. C*, 2008, **112**, 8951.
- 42 S. Livraghi, M. Chiesa, M.C. Paganini and E. Giamello, *J. Phys. Chem. C*, 2011, **115**, 25413.
- 43 O. Micic, Y. Zhang, C. Cromack, A. Trifunac and M. Thurnauer, *J. Phys. Chem*, 1993, **97**, 1211.
- 44 a) D. C. Hurum, A. G. Agrios, K. A. Gray, T. Rajh, M. Thurnauer, *J. Phys. Chem. B*, 2003, **107**, 4545; b) D. C. Hurum, K. A. Gray, T. Rajh and M. Thurnauer, *J. Phys. Chem. B*, 2005, **109**, 977; d) D. C. Hurum, A. G. Agrios, S. E. Crist, K. A. Gray, T. Rajh and M. Thurnauer, *J. Electron Spectroscopy and Related Phenomena* 2006, 150, 155.
- 45 P.F. Chester, *J. Appl. Phys.*, 1961, **32**, 866.
- 46 P.H. Zimmerman, *Phys. Rev. B*, 1973, **8**, 3917.
- 47 D. L. Griscom *Phys Rev. B*, 1989, **40**, 4224.
- 48 C. Gionco, M.C. Paganini, E. Giamello, unpublished work.
- 49 M. Chiesa, M. C. Paganini, E. Giamello, D. M. Murphy, C. Di Valentin and G. Pacchioni, *Acc. Chem. Res.*, 2006, **39**, 861.
- 50 T. Berger, O. Diwald, E. Knoezinger, F. Napoli, M. Chiesa and E. Giamello, *Chem. Phys.*, 2007, **339**, 138.
- 51 T. Rajh, A.E. Ostafin, O. I. Micic, D. M. Tiede and M. C. Thurnauer, *J. Phys. Chem.*, 1996, **100**, 4538.
- 52 a) M. A. Henderson, *Surf. Sci.*, 1995, **343**, L1156–L1160; b) M. A. Henderson, *Surf. Sci.*, 1999, **419**, 174.
- 53 M. Li, W. Hebenstreit, U. Diebold, A. M. Tyryshkin, M.K. Bowman, G. G. Dunham and M. A. Henderson, *J. Phys. Chem. B*, 2000, **104**, 4944.
- 54 M. Aono and R. R. Hasiguti, *Phys. Rew. B.*, 1993, **48**, 12406.
- 55 M. Xing, W. Fang, M. Nasir, Y. Maa, J. Zhang and M. Anpo *J. Catal.*, 2013, **297**, 236; Fan Zuo, L. Wang, T. Wu, Z. Zhang, D. Borchardt and Pingyun Feng, *J. Am. Chem. Soc.* 2010, **132**, 11856; T. R. Gordon, M. Cargnello, T. Paik, F. Mangolini, T. Weber, P. Fornasiero and C. B. Murray, *J. Am. Chem. Soc.* 2012, 134, 6751.
- 56 S. Livraghi, S. Maurelli, M.C. Paganini, M. Chiesa and E. Giamello, *Angew. Chem Intern. Ed.*, 2011, **50**, 8038.
- 57 S. D. Eliot and S. P. Bates, *Phys. Chem. Chem. Phys.*, 2001, **3**, 1954.
- 58 E. Finazzi, C. Di Valentin and G. Pacchioni, *J. Phys. Chem. C*, 2009, **113**, 3382.
- 59 a) M. Chiesa, P. Martino, E. Giamello, C. Di Valentin and G. Pacchioni, *J. Phys. Chem. B* 2004, **108**, 11529; b) M. Chiesa, E. Giamello, C. Di Valentin, G. Pacchioni, Z. Sojka and S. Van Doorslaer, *J. Am. Chem., Soc.* 2005, **127**, 16935. c) M. Chiesa, M. C. Paganini, E. Giamello, C. Di Valentin and G. Pacchioni, *ChemPhysChem*, 2006, **7**, 728.
- 60 J. K. Burdett, *Inorg. Chem.*, 1985, **24**, 2244.
- 61 D. Baute and D. Goldfarb, *J. Phys. Chem, A*, 2005, **109**, 7865.
- 62 S. Maurelli, S. Livraghi, M. Chiesa, E. Giamello, S. Van Doorslaer, C. Di Valentin and G. Pacchioni, *Inorg. Chem.*, 2011, **50**, 2385.
- 63 H. Tang, K. Prasad, R. Sanjines, P. E. Schmid and F. Lévy, *J. Appl. Phys.*, 1994, **75**, 2042.